

## CONNECTING REIONIZATION TO THE LOCAL UNIVERSE

MARCELO A. ALVAREZ, MICHAEL BUSH, TOM ABEL, AND RISA H. WECHSLER  
Kavli Institute for Particle Astrophysics and Cosmology, Stanford University, Menlo Park, CA 94025  
*Draft version October 29, 2018*

### ABSTRACT

We present results of combined N-body and three-dimensional reionization calculations to determine the relationship between reionization history and local environment in a volume  $1 \text{ Gpc } h^{-1}$  across and a resolution of about  $1 \text{ Mpc}$ . We resolve the formation of about  $2 \times 10^6$  halos of mass greater than  $\sim 10^{12} M_{\odot}$  at  $z = 0$ , allowing us to determine the relationship between halo mass and reionization epoch for galaxies and clusters. For our fiducial reionization model, in which reionization begins at  $z \sim 15$  and ends by  $z \sim 6$ , we find a strong bias for cluster-size halos to be in the regions which reionized first, at redshifts  $10 < z < 15$ . Consequently, material in clusters was reionized within relatively small regions, on the order of a few Mpc, implying that all clusters in our calculation were reionized by their own progenitors. Milky Way mass halos were on average reionized later and by larger regions, with a distribution most similar to the global one, indicating that low mass halos are nearly uncorrelated with reionization when only their mass is taken as a prior. On average, we find that most halos with mass less than  $10^{13} M_{\odot}$  were reionized internally, while almost all halos with masses greater than  $10^{14} M_{\odot}$  were reionized by their own progenitors. We briefly discuss the implications of this work in light of the “missing satellites” problem and how this new approach may be extended further.

*Subject headings:* cosmology: theory — galaxies: formation — galaxies: intergalactic medium

### 1. INTRODUCTION

The universe we observe at  $z = 0$  must bear the marks of reionization. Reionization began when the first stars polluted the intergalactic medium and created individual H II regions (Alvarez et al. 2006; Abel et al. 2007; Yoshida et al. 2007; Wise & Abel 2008). As the first galaxies grew in abundance, the H II regions became longer lived, eventually containing perhaps tens of thousands of dwarf galaxies, growing and merging until they overlapped, marking the end of reionization (Shapiro & Giroux 1987; Miralda-Escudé et al. 2000; Gnedin 2000a; Sokasian et al. 2001; Nakamoto et al. 2001; Ciardi et al. 2003; Furlanetto et al. 2004; Iliiev et al. 2006; Zahn et al. 2007; Trac & Cen 2007). Observations of high-redshift quasars imply that this process was complete by redshift  $z \sim 6$  (Becker 2001; Fan et al. 2002; White et al. 2003; Willott 2007), while large-angle polarization measurements of the cosmic microwave background constrain the duration of reionization (Spergel 2003; Komatsu 2008).

During this time, the temperature of the intergalactic medium increased from a few to tens of thousands of degrees, dramatically changing the evolution of gas as it responded to the highly dynamic underlying dark matter potential.

Low mass halos in ionized regions are less able cool, collapse, and form stars than those in neutral regions, due to the increase in the cosmological Jeans mass when gas is ionized and photo-heated, sometimes called “Jeans mass filtering” (e.g., Shapiro et al. 1994; Thoul & Weinberg 1996; Gnedin 2000b; Dijkstra et al. 2004; Shapiro et al. 2004). This suppression of structure is one of the fundamental ways that reionization can leave its imprint on subsequent structure formation, even up until the present day.

Correlating reionization with the present-day environment may be the key to the so-called “missing satellite problem” — many more satellite halos are predicted to form in CDM than are actually observed as galaxies (Klypin et al. 1999). The leading explanation — an alternative to more exotic possibil-

ities like modifying dark matter or the amplitude of small-scale primordial density fluctuations — is that the UV background maintains the intergalactic gas in a photo-heated state, preventing it from falling into the shallow potential wells of the progenitors of the satellite halos (e.g., Bullock et al. 2000; Benson et al. 2002). For example, one might expect that regions that were reionized earlier will have fewer luminous satellites than regions that were ionized later. However, biased regions, which are rich in early low-mass galaxy formation, would have reionized *first*. The latter effect implies that early reionization would lead to more satellite galaxies, while the former implies just the opposite. Detailed three-dimensional models are necessary in order to disentangle these competing effects and quantify their dependence on the inevitable assumptions that must be made when modeling reionization on such large scales.

In this *Letter*, we present our first calculations to address the correlation between reionization and local environment. We take a novel approach, combining N-body simulations with a “semi-numerical” algorithm (Zahn et al. 2007; Mesinger & Furlanetto 2007) for calculating the reionization history for the simulation, allowing us to achieve a higher dynamic range in resolving the scales of reionization than has been possible until now. We then report on the statistical correlations between halo properties and their reionization epoch and environment. We present our hybrid N-body/semi-numerical method in §2, our results in §3, and end with a discussion in §4. Throughout, we assume a flat universe with  $\Omega_m = 0.25$ ,  $\sigma_8 = 0.8$ ,  $n_s = 1$ ,  $\Omega_b = 0.04$ , and  $h = 0.7$ .

### 2. MODEL

Our hybrid approach consists of two steps. First, we run an N-body simulation of structure formation to determine the positions and masses of halos at  $z = 0$ . We then calculate the reionization history of the same volume in order to determine the reionization epoch of each halo.

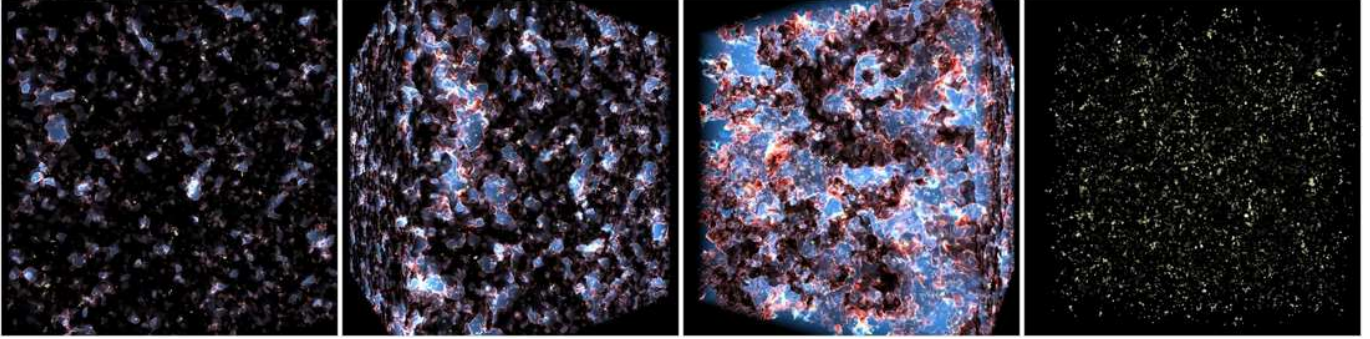


FIG. 1.— Visualization of the progress of reionization in our  $1 \text{ Gpc} h^{-1}$  calculation. Redshifts  $z = 14$ ,  $z = 10$ ,  $z = 8$ , and  $z = 6$  are shown from right to left. Ionized regions are blue and translucent, ionization fronts are red and white, and neutral regions are dark and opaque. A random sampling of 5 per cent (about 40,000) of all the halos at  $z = 0$  are shown in yellow. Reionization is still quite inhomogeneous on these large scales, with large regions ionizing long before others.

### 2.1. *N-body Dark Matter Simulations*

For our cosmological N-body simulations, we used the code GADGET-2 (Springel 2005). We simulated a periodic box  $1 \text{ Gpc}/h$  on a side with  $1120^3$  N-body particles. We did not include any gas dynamics, a reasonable choice given that we are interested only in the global properties of the dark matter halos, not the internal properties of the baryonic component. We used a comoving softening length of  $25 \text{ kpc}$ , sufficient to resolve the formation of halos of mass  $\sim 10^{12} M_{\odot}$ . At  $z = 0$  we use a friends-of-friends halo finder with a linking length of  $0.2$  mean inter-particle spacings to identify the halos.

### 2.2. *Semi-numerical Reionization*

Our model is based on the analytical formalism first introduced by Furlanetto et al. (2004) and later extended to three dimensional realizations by Zahn et al. (2007). Its main assumption is that a region is fully ionized if its collapse fraction, defined as the fraction of matter present in halos above some minimum mass  $M_{\min}$ , is greater than some threshold,

$$\zeta f_{\text{coll}} > 1. \quad (1)$$

This corresponds, for example, to the assumption that  $\zeta \dot{f}_{\text{coll}}$  ionizing photons are released per atom per unit time. If recombinations are neglected, then equation (1) results by ensuring that the time-integrated number of ionizing photons released is greater than the number of the atoms. Another interpretation of the efficiency factor  $\zeta$  is that each halo produces a spherical ionized region around it, the size of which is directly proportional to its mass. Thus, all the recombination, and radiative transfer physics is absorbed into our choice of  $\zeta$ . For example,  $\zeta = (f_{\text{esc}} f_* N_{\gamma/b}) / (1 + n_{\text{rec}})$  where  $f_{\text{esc}}$  is the escape fraction of ionizing photons from each halo,  $f_*$  is the fraction of matter converted to stars within a halo,  $N_{\gamma/b}$  is the number of ionizing photons produced in stars per hydrogen atom,  $n_{\text{rec}}$  is the average number of recombinations per hydrogen atom during reionization (Furlanetto et al. 2004).

To apply this criterion for “self-ionization” to an actual three-dimensional linear density field, we use the following relation for the collapsed fraction within a spherical region of mass  $m$  and density contrast  $\delta$  (Lacey & Cole 1993):

$$f_{\text{coll}} = \text{erfc} \left[ \frac{\delta_c(z) - \delta_m}{\sqrt{2[\sigma^2(M_{\min}) - \sigma^2(m)]}} \right], \quad (2)$$

where  $\sigma^2(m)$  is the mass variance over the scale  $m$ ,  $\delta_c(z)$  is the critical density for collapse, and  $M_{\min}$  is the minimum mass of

halos to be counted in the collapsed fraction, i.e. the minimum mass of a halo capable of producing a significant amount of photoionizing radiation. Note that the time dependence of the density field has been taken into account in the critical density for collapse,  $\delta_c(z) = \delta_{c,0}/D(z)$ , where  $D(z)$  is the linear growth factor, so that  $\sigma(m)$  and  $\delta_m$  are constant in time. As shown by Furlanetto et al. (2004), this results in a time and scale-dependent “barrier” around each point,

$$\delta_m \geq \delta_x(m, z) \equiv \delta_c(z) - \sqrt{2} [\sigma^2(M_{\min}) - \sigma^2(m)]^{1/2} \text{erf}^{-1}(1 - \zeta^{-1}). \quad (3)$$

The mean density within a sphere around a given point,  $\delta_m$ , must be greater than this barrier,  $\delta_x(m, z)$ , in order for the point at the center to be ionized by that region. A given point is considered to be ionized when the condition in equation 3 is met for *any* smoothing scale  $m$ , so that

$$z_{\text{reion}} = \text{MIN}_m \left[ D_0 \left( \delta_m + \sqrt{2} \text{erf}^{-1}(1 - \zeta) [\sigma^2(m_{\min}) - \sigma^2(m)] \right) - 1 \right], \quad (4)$$

where  $\text{MIN}_m$  indicates the minimum value over all smoothing scales  $m$ .

In practice, the outcome of this modeling is one value of  $z_{\text{reion}}$  at each point on the grid, which characterizes the evolution of reionization over all time. The smoothing of the density field over all scales can be accomplished through a fast Fourier transform (FFT). We also store the radius at which each point on the grid first crossed the barrier, and associate it with it with the characteristic size of the region containing the sources that first ionized the grid point.

Finally, to associate with each  $z = 0$  halo a reionization epoch and H II region size, we assign each of them a value that corresponds to the cell in which its center of mass lies at present. Given that typical H II regions are tens of Mpc, the vast majority of halos in our volume would not have had the required sustained peculiar velocities in excess of  $10^3 \text{ km/s}$  for 10 Gyrs to have moved out of such a region. We thus expect our results to be robust for most halos in the box, with the predictions being least accurate for the few halos that are just on the verge of falling into large galaxy clusters. Here, the reionization epochs could be overestimated, and H II region sizes underestimated. We set the parameters of the reionization model to have a minimum halo mass of  $M_{\min} = 10^8 M_{\odot}$  and an efficiency parameter  $\zeta = 10$ .

## 3. RESULTS

Figure 1 shows snapshots of the reionization calculation at four different times for a  $1024^3$  grid. Even on scales of 100

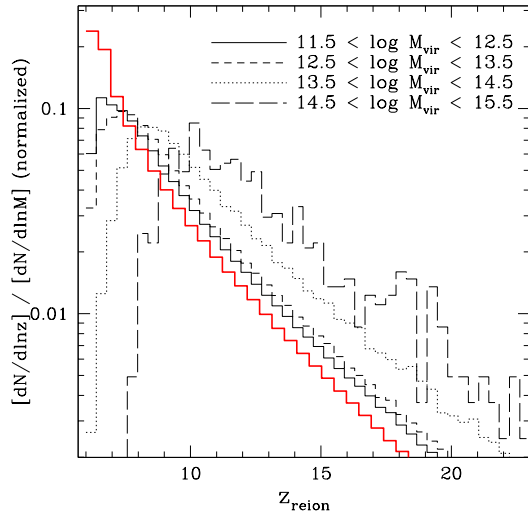


FIG. 2.— Reionization redshift distributions, for the regions that became halos in different mass intervals (see labels) by redshift zero. A uniform binning was used in redshift, with the same spacing for each of the mass ranges. The low-mass distributions are very well sampled because of their large numbers, while the high-mass halos, especially at the cluster scale, become noisy, owing to their small number (only 800 even in a  $1 \text{ Gpc}h^{-1}$  box). The thick red line shows the distribution for random points in the box.

Mpc, reionization remains inhomogeneous, with the reionization redshift of regions as large as tens of Mpc varying between  $z_r \sim 15$  and  $z_r \sim 6$ . Although regions that were reionized first are at the peaks of the underlying density field, there is not a one-to-one correspondence between the mass of the  $z = 0$  halos and their reionization epochs, since the halo and reionization barrier shapes and amplitudes differ.

Figure 2 shows the distribution of halo reionization epochs, for several ranges of halo mass. There is considerable spread in reionization redshifts in this model, ranging over  $6 < z_r < 15$ . The most massive halos are biased toward higher values of  $z_r$ , peaking at  $z \sim 10$ , 8, and 7 for masses  $M \sim 10^{15}$ ,  $10^{14}$ , and  $10^{13} M_\odot$ . The distribution of the lowest mass halos, with masses  $\sim 10^{12} M_\odot$ , does not have a well-defined peak, but rather increases toward the lowest redshifts, peaking at the percolation epoch at  $z \sim 6$ . This indicates that these lowest mass halos are relatively unbiased with respect to the structure of reionization.

Figure 4 shows the 68 and 95 per cent contours of the reionization redshift distribution for halos binned by their mass. The median value increases from  $z_r \simeq 8$  for  $M_h = 10^{12} M_\odot$ , to  $z \simeq 12$  for  $M_h = 10^{15} M_\odot$ . The distributions have a long tail toward higher reionization values, which is more pronounced for higher-mass halos. Only 5 percent of  $10^{12} M_\odot$  halos have  $z_r > 12$ , while only 5 percent of cluster scale halos have  $z_r < 8$ . Such a large spread in reionization epochs at all masses implies that other halo properties, such as merger history and local matter density, may be important in setting the reionization epoch for a specific halo such as our own Milky Way.

The mass-dependent distributions of bubble sizes are shown in Figure 3. Lower mass halos largely form in regions with larger H II bubbles, since their sizes increase with time. Interestingly, all of the roughly 800 cluster-mass halos in our sample are associated with H II region sizes less than 30 Mpc. Only halos below about  $10^{13} M_\odot$  have H II regions sizes in excess of 100 Mpc, exceeding the mean free path for Lyman-limit systems and approaching (and potentially exceeding) the

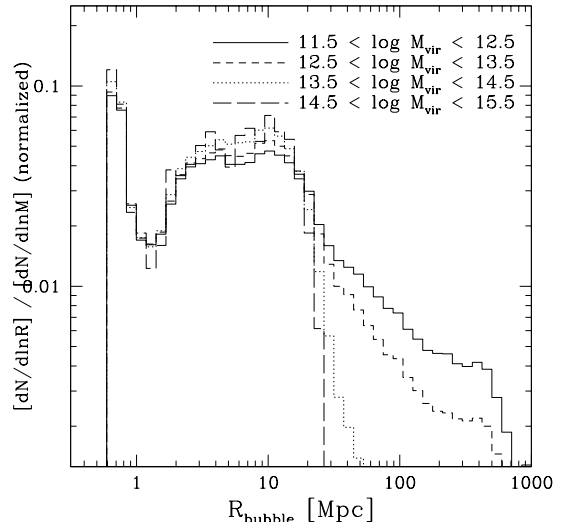


FIG. 3.— H II region sizes at reionization for the same mass bins as Figure 2. The peak at low masses can be attributed to the grid resolution, given by a radius of  $\sim 0.5$  Mpc. Increased resolution would reduce the effect, but on such small scales the role of recombinations and the stochasticity of the sources are likely to play an increasing role, effects we have not yet self-consistently included in these calculations. The distribution at scales larger than  $\sim 1$  Mpc are robust predictions of our model.

size of the box,  $1 \text{ Gpc}h^{-1}$ .

#### 4. DISCUSSION

Using large-volume and high-resolution coupled simulations of reionization and halo formation, we have developed a new method for connecting the  $z = 0$  distribution of halos to the reionization epoch. We have found that, when only their mass is known, galaxy scale halos are nearly uncorrelated with respect to reionization, with a distribution of H II region bubble sizes and reionization epochs that are roughly consistent with having a random spatial distribution. Higher mass halos, however, show a much stronger correlation, with none of the cluster scale objects having  $z_r < 8$  or  $R_{\text{HII}} > 30$  Mpc.

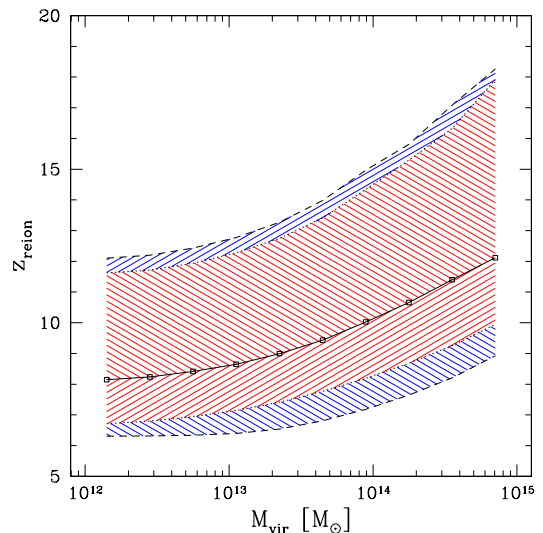


FIG. 4.— Median (solid line) and spread in the values of the reionization redshift,  $z_{\text{reion}}$ , as a function of halo mass. Shaded contours indicate the 68 per cent (red) and 95 per cent (blue) spread in the distribution. The higher the halo mass today the earlier its progenitors were likely reionized.

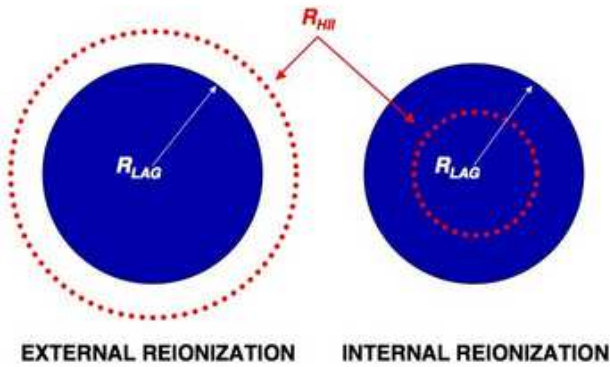


FIG. 5.— Schematic diagram indicating the difference between external and internal reionization.  $R_{HII}$  indicates the size of the reionizing bubble;  $R_{Lag}$  indicates the Lagrangian radius of the halo.

An important distinction is between *internal* and *external* reionization. Figure 5 describes these two possibilities. In the external reionization case, the halo material was ionized by sources in a region with  $R_{HII} \gg R_{Lag}$ , where  $R_{Lag}$  is the co-moving volume occupied by the mass of the halo at the cosmic mean density. In this case, most of the sources that ionized the material were not progenitors of the halo, and the ionization front swept over the halo’s progenitors quickly, leaving the halo with a relatively uniform reionization epoch. For internal reionization,  $R_{HII} \ll R_{Lag}$ , and the halo’s reionization history is likely to be much more complex. In general, more massive halos were internally reionized, while less massive ones were externally reionized.

Our definition is somewhat different from previous definitions (e.g., Weinmann et al. 2007), but we believe our definition is best suited for the method used here. In our definition, halos are considered to be externally ionized if their Lagrangian radius, defined by  $M_{halo} = 4\pi\bar{\rho}R_{Lag}^3/3$ , is smaller than their H II region radius. For galaxy scale objects, with Lagrangian radii of order 2 Mpc, it is clear from Figure 3 that most of these objects were externally ionized. Because our model does not resolve scales below about a Mpc, however, it is difficult to determine how few galaxies were internally ionized. More detailed modeling of the small-scale structure on galactic scales, while still retaining the large volume presented here, is therefore necessary. Our predictions for clusters are more robust. For these objects, with Lagrangian radii of order 20 Mpc, all but a tiny handful are internally ionized.

Our results may have important implications for galaxy formation, and in particular for the missing satellites problem. Because we find such a large spread in reionization epochs for Milky Way mass halos, more information, such as larger-scale environment and accretion history, will be necessary to determine the reionization epoch of our own halo, even after the global reionization history is well constrained. If the abundance of Galactic satellites is strongly dependent on the reionization epoch of the galaxy, our results indicate that Milky Way mass halos would have a large spread in the number of observable satellites. We explore this issue in a companion paper (Busha et al., in preparation).

Our results may also have implications for the issue of galaxy “assembly bias”, the idea that galaxy clustering may be dependent on properties other than the mass of their host halos (Wechsler et al. 2006; Gao & White 2007; Croton et al. 2007). If the reionization epoch of halos at a given mass is correlated with halo formation time, and if the reionization epoch affects any aspects of the galaxy population, then assembly bias could be more important for such galaxies than it is for their host halos. Further study will be required to investigate such effects.

The approach we have presented here will serve as the foundation for such more detailed future studies. These studies will investigate the statistical correlations between present-day structure and reionization, and will also incorporate detailed galaxy formation modeling. Such improvements will allow for an investigation of the detailed coupling between star formation histories and the local reionization history.

This work was partially supported by NASA AITP grant NNX08AH26G and NSF AST-0807312. RHW was supported by a Terman Fellowship at Stanford University. We thank Louis Strigari for discussion about the missing satellite problem. MAA thanks Ilian Iliev and Piero Madau for helpful discussions. The Gpc simulation was performed on the Orange cluster at SLAC as a part of the LasDamas project; MTB and RHW thank their collaborators on the LasDamas project (<http://lss.phy.vanderbilt.edu/lasdamas/>) for critical input. We are grateful for the continuous support from the SLAC computational team.

#### REFERENCES

- Abel, T., Wise, J. H., & Bryan, G. L. 2007, *ApJ*, 659, L87  
 Alvarez, M. A., Bromm, V., & Shapiro, P. R. 2006, *ApJ*, 639, 621  
 Becker, R. H. e. a. 2001, *AJ*, 122, 2850  
 Benson, A. J., Frenk, C. S., Lacey, C. G., Baugh, C. M., & Cole, S. 2002, *MNRAS*, 333, 177  
 Bullock, J. S., Kravtsov, A. V., & Weinberg, D. H. 2000, *ApJ*, 539, 517  
 Ciardi, B., Stoehr, F., & White, S. D. M. 2003, *MNRAS*, 343, 1101  
 Croton, D. J., Gao, L., & White, S. D. M. 2007, *MNRAS*, 374, 1303  
 Dijkstra, M., Haiman, Z., Rees, M. J., & Weinberg, D. H. 2004, *ApJ*, 601, 666  
 Fan, X., Narayanan, V. K., Strauss, M. A., White, R. L., Becker, R. H., Pentericci, L., & Rix, H.-W. 2002, *AJ*, 123, 1247  
 Furlanetto, S. R., Zaldarriaga, M., & Hernquist, L. 2004, *ApJ*, 613, 1  
 Gao, L. & White, S. D. M. 2007, *MNRAS*, 377, L5  
 Gnedin, N. Y. 2000a, *ApJ*, 535, 530  
 —. 2000b, *ApJ*, 542, 535  
 Iliev, I. T., Mellema, G., Pen, U.-L., Merz, H., Shapiro, P. R., & Alvarez, M. A. 2006, *MNRAS*, 369, 1625  
 Klypin, A., Kravtsov, A. V., Valenzuela, O., & Prada, F. 1999, *ApJ*, 522, 82  
 Komatsu, E. e. a. 2008, *ArXiv e-prints*  
 Lacey, C. & Cole, S. 1993, *MNRAS*, 262, 627  
 Mesinger, A. & Furlanetto, S. 2007, *ApJ*, 669, 663  
 Miralda-Escudé, J., Haehnelt, M., & Rees, M. J. 2000, *ApJ*, 530, 1  
 Nakamoto, T., Umemura, M., & Susa, H. 2001, *MNRAS*, 321, 593  
 Shapiro, P. R. & Giroux, M. L. 1987, *ApJ*, 321, L107  
 Shapiro, P. R., Giroux, M. L., & Babul, A. 1994, *ApJ*, 427, 25  
 Shapiro, P. R., Iliev, I. T., & Raga, A. C. 2004, *MNRAS*, 348, 753  
 Sokasian, A., Abel, T., & Hernquist, L. E. 2001, *New Astronomy*, 6, 359  
 Spergel, D. N. e. a. 2003, *ApJS*, 148, 175  
 Springel, V. 2005, *MNRAS*, 364, 1105  
 Thoul, A. A. & Weinberg, D. H. 1996, *ApJ*, 465, 608  
 Trac, H. & Cen, R. 2007, *ApJ*, 671, 1  
 Wechsler, R. H., Zentner, A. R., Bullock, J. S., Kravtsov, A. V., & Allgood, B. 2006, *ApJ*, 652, 71  
 Weinmann, S. M., Macciò, A. V., Iliev, I. T., Mellema, G., & Moore, B. 2007, *MNRAS*, 381, 367  
 White, R. L., Becker, R. H., Fan, X., & Strauss, M. A. 2003, *AJ*, 126, 1  
 Willott, C. J. e. a. 2007, *AJ*, 134, 2435  
 Wise, J. H. & Abel, T. 2008, *ApJ*, 684, 1  
 Yoshida, N., Oh, S. P., Kitayama, T., & Hernquist, L. 2007, *ApJ*, 663, 687  
 Zahn, O., Lidz, A., McQuinn, M., Dutta, S., Hernquist, L., Zaldarriaga, M., & Furlanetto, S. R. 2007, *ApJ*, 654, 12